# Mobile zinc increases rapidly in the retina after optic nerve injury and regulates ganglion cell survival and optic nerve regeneration

Yiqing Li[a,b,c], Lukas Andereggen[a,c], Kenya Yuki[a,c], Kumiko Omura[a,c], Yuqin Yin[a,c], Hui-Ya Gilbert[a,c], Burcu Erdogan[a], Maria S. Asdourian[a], Christine Shrock[a], Silmara de Lima[a,c], Ulf-Peter Apfel[d], Yehong Zhuo[b], Michal Hershfinkel[e], Stephen J. Lippard[d], Paul A. Rosenberg[c,f,g,1,2], and Larry Benowitz[a,c,g,h,1,2]

[a]Department of Neurosurgery, Boston Children's Hospital and Harvard Medical School, Boston, MA 02115; [b]State Key Laboratory of Ophthalmology, Zhongshan Ophthalmic Center, Sun Yat-sen University, Guangzhou 510060, China; [c]F.M. Kirby Neurobiology Center, Boston Children's Hospital, Boston, MA 02115; [d]Department of Chemistry, Massachusetts Institute of Technology, Cambridge, MA 02139; [e]Department of Physiology and Cell Biology, Faculty of Health Sciences, Ben-Gurion University of the Negev, Beer-Sheva 84105, Israel; [f]Department of Neurology, Boston Children's Hospital and Harvard Medical School, Boston, MA 02115; [g]Program in Neuroscience, Harvard Medical School, Boston, MA 02115; and [h]Department of Ophthalmology, Harvard Medical School, Boston, MA 02115

Edited by David J. Calkins, Vanderbilt University Medical Center, Nashville, TN, and accepted by Editorial Board Member Jeremy Nathans November 29, 2016 (received for review October 13, 2016)

**Retinal ganglion cells (RGCs), the projection neurons of the eye, cannot regenerate their axons once the optic nerve has been injured and soon begin to die. Whereas RGC death and regenerative failure are widely viewed as being cell-autonomous or influenced by various types of glia, we report here that the dysregulation of mobile zinc ($Zn^{2+}$) in retinal interneurons is a primary factor. Within an hour after the optic nerve is injured, $Zn^{2+}$ increases several-fold in retinal amacrine cell processes and continues to rise over the first day, then transfers slowly to RGCs via vesicular release. $Zn^{2+}$ accumulation in amacrine cell processes involves the $Zn^{2+}$ transporter protein ZnT-3, and deletion of *slc30a3*, the gene encoding ZnT-3, promotes RGC survival and axon regeneration. Intravitreal injection of $Zn^{2+}$ chelators enables many RGCs to survive for months after nerve injury and regenerate axons, and enhances the prosurvival and regenerative effects of deleting the gene for phosphatase and tensin homolog (*pten*). Importantly, the therapeutic window for $Zn^{2+}$ chelation extends for several days after nerve injury. These results show that retinal $Zn^{2+}$ dysregulation is a major factor limiting the survival and regenerative capacity of injured RGCs, and point to $Zn^{2+}$ chelation as a strategy to promote long-term RGC protection and enhance axon regeneration.**

exocytosis | amacrine cell | chelation | neuroprotection | cell death

The optic nerve has been widely used to investigate the response of CNS neurons to injury because of its accessibility, anatomy, and functional importance. Under normal circumstances, retinal ganglion cells (RGCs), the projection neurons of the eye, cannot regenerate axons after the optic nerve has been damaged and soon undergo cell death, leaving victims of traumatic or ischemic nerve injury or degenerative conditions, such as glaucoma, with permanent visual losses. Optic nerve injury leads to numerous pathological changes in RGCs and reversing some of these changes improves cell survival, although these effects are often transitory and for the most part promote little or no axon regeneration (1–10). Regeneration per se can be induced by intraocular inflammation combined with elevated cAMP (11, 12), counteracting cell-intrinsic (13–15) or cell-extrinsic (16, 17) suppressors of axon growth, oncomodulin and other growth factors (18–22), or elevated physiological activity (23, 24). Some of these treatments act synergistically and enable a modest number of RGCs to reestablish connections with appropriate target areas in the brain (25–27). However, although these studies show that successful regeneration can occur in principle, most RGCs eventually die after optic nerve injury, and to date only a small fraction of surviving RGCs have been induced to regenerate axons (27). These observations imply the existence of other major, as yet unknown suppressors of cell survival and regeneration. Our results point to zinc dysregulation as a critical factor.

Zinc is essential for many cellular functions. Covalently bound zinc is required for the activity of numerous enzymes and transcription factors (28). The zinc finger is an ancient structural motif capable of interacting with both DNA and RNA, and proteins containing this motif are the most-abundant class of proteins in the human proteome (29). Mobile or chelatable zinc ($Zn^{2+}$) is concentrated in synaptic vesicles and other intracellular organelles (30) but is otherwise maintained in the cytoplasm at concentrations of $\sim 10^{-10}$ M (31–33). $Zn^{2+}$ can be liberated from metallothionein and intracellular organelles or can enter cells through voltage-gated $Ca^{2+}$ channels, $Ca^{2+}$- permeable glutamate receptors, transient receptor potential channels, and specific $Zn^{2+}$ transporters (30, 34–36). Synaptic $Zn^{2+}$ plays an essential role in modulating synaptic transmission throughout the brain (37–40), including the retina, where it contributes to neuromodulation and neuroprotection (41, 42). Zinc nutritional deficiency or cellular deficiency as a result of mutation in zinc transporters produces

## Significance

**The inability of CNS pathways to regenerate after injury can lead to devastating, life-long losses in sensory, motor, and other functions. We report that after injury to the optic nerve, a widely studied CNS pathway that normally cannot regenerate, mobile zinc ($Zn^{2+}$) increases rapidly in the processes of retinal interneurons (amacrine cells) and then transfers via vesicular release to retinal ganglion cells (RGCs), the injured projection neurons. Eliminating $Zn^{2+}$ leads to both persistent RGC survival and substantial axon regeneration with a broad therapeutic window. These findings show that signaling between interneurons and RGCs contributes to regulating the fate of RGCs after optic nerve injury, and that $Zn^{2+}$ chelation may provide a potent therapeutic approach.**

Author contributions: Y.L., P.A.R., and L.B. designed research; Y.L., L.A., K.Y., K.O., Y.Y., H.-Y.G., B.E., M.S.A., C.S., and S.d.L. performed research; U.-P.A., Y.Z., M.H., and S.J.L. contributed new reagents/analytic tools; Y.L., L.A., K.Y., Y.Y., and H.-Y.G. analyzed data; and Y.L., L.A., P.A.R., and L.B. wrote the paper.

The authors declare no conflict of interest.

This article is a PNAS Direct Submission. D.J.C. is a Guest Editor invited by the Editorial Board.

[1]P.A.R. and L.B. contributed equally to this work.

[2]To whom correspondence may be addressed. Email: paul.rosenberg@childrens.harvard.edu or larry.benowitz@childrens.harvard.edu.

This article contains supporting information online at www.pnas.org/lookup/suppl/doi:10.1073/pnas.1616811114/-/DCSupplemental.

significant human disability (43–46). Zinc also contributes to neuronal death in hypoxic-ischemic injury (34, 35, 47–49) by interfering with mitochondrial and metabolic functions (50, 51), altering ion fluxes (52), and other mechanisms (53). Abnormalities in zinc homeostasis may be important in chronic neurodegenerative diseases, such as Alzheimer's (54) and amyotrophic lateral sclerosis (55–57), and have been shown to play a key role in oxidative stress-induced death in neurons and oligodendrocytes (58, 59). Given the abundant evidence for the importance of zinc in acute and chronic neurodegeneration, we have investigated its involvement in the death of RGCs following optic nerve injury. We show here that $Zn^{2+}$ accumulates in amacrine cell processes shortly after optic nerve injury before being transferred to RGCs, and that $Zn^{2+}$ chelation allows many injured RGCs to survive for months. Remarkably, $Zn^{2+}$ chelation also provides a strong stimulus for axon regeneration.

## Results

**$Zn^{2+}$ Increases in the Inner Retina Shortly After Optic Nerve Crush.** Most of our studies used autometallography (AMG) (60) to visualize $Zn^{2+}$ in the retina because of the selectivity of this method for $Zn^{2+}$ per se, its utility for semiquantitative studies, the stability of the reaction product, and high level of reproducibility (61, 62). Whereas AMG revealed only modest levels of $Zn^{2+}$ in the normal retina, by 6 h after optic nerve crush (NC), the earliest time point we examined using AMG (*Methods*), the $Zn^{2+}$ signal in the inner plexiform layer (IPL) was 4.4 ± 0.3-fold above baseline (mean ± SEM) (Fig. 1 *A*, *B*, and *D*) and continued to rise over the next 18 h (Fig. 1 *B* and *D*). Staining was particularly prominent in the inner- and outermost sublaminae of the IPL. Although our standard staining protocol showed little signal in the normal retina, extending the development time revealed definite $Zn^{2+}$ AMG staining (Fig. S1 *A* and *B*), in agreement with earlier studies (41, 63). Quantitatively, the staining intensity in the IPL after NC relative to that of the intact retina was largely insensitive to the reaction time over a range of 0.5–3 h (Fig. S1 *A* and *B*). The IPL in the retina contralateral to the injured optic nerve showed a small, transient elevation of $Zn^{2+}$ (Fig. S2 *A–C*), reminiscent of other contralateral effects reported after unilateral optic nerve injury (64). Because the contralateral signal changes over time, we used the normal, intact retina as a reference throughout the study, always staining control and experimental retinas together.

After 2–3 d, whereas the $Zn^{2+}$ signal in the IPL had declined, cells within the ganglion cell layer (GCL) showed strong staining (Fig. 1 *B* and *E* and Fig. S1 *C* and *D*). To investigate whether the AMG signal accurately reflected $Zn^{2+}$, we tested whether it could be eliminated by the high-affinity, membrane-permeable $Zn^{2+}$ chelator TPEN [N,N,N′,N′-tetrakis(2- pyridyl methyl) ethylenediamine] (65) or the recently developed, highly selective, membrane-impermeable $Zn^{2+}$ chelator ZX1 (38). A single intraocular injection of either TPEN or ZX1 immediately after NC eliminated the AMG signal in the IPL when examined at 6 h and 1 d (Fig. 1 *B* and *D* and Fig. S1*E*) and strongly suppressed, but did not fully eliminate, the IPL signal and the number of positively stained cells in the GCL at 2–3 d (Fig. S1*F*).

We extended these results by using the membrane-permeable, highly selective fluorescent $Zn^{2+}$ sensor Zinpyr-1 (ZP-1) (38, 66), which affords higher spatial and temporal resolution than AMG. By 1 h after NC, the ZP-1 signal in the IPL was 2.8 ± 0.3-fold above baseline (mean ± SEM; Bonferroni-corrected $P = 0.036$) and continued to rise over the first 24 h (Fig. 1 *C* and *F*). In agreement with the AMG results, the ZP-1 signal in the IPL declined by 3 d while becoming strongly elevated in cells of the GCL (Fig. 1*C*). ZX1 and TPEN both eliminated the ZP-1 signal at 6 h, verifying its association with $Zn^{2+}$ per se (Fig. 1*F*) (all Bonferroni-corrected $P < 0.0001$). The nearly identical changes in $Zn^{2+}$ levels observed in the retina over time using two completely different methods further validates the use of AMG for semiquantitative studies. Intraocular injection of inorganic $Zn^{2+}$ ($ZnCl_2$, 100 μM, 1 mM) failed to elevate the $Zn^{2+}$-AMG signal in the retina (Fig. S2 *D–F*) and did not impair RGC survival (Fig. S2 *G* and *H*), although we do not know how well exogenous $Zn^{2+}$ reaches the neural retina nor whether it enters cells in the absence of nerve injury or manipulations that open zinc permeation pathways.

**$Zn^{2+}$ Accumulation Requires the Zinc Transporter Protein ZnT-3.** ZnT-3 loads $Zn^{2+}$ into synaptic vesicles of glutamatergic, monoaminergic, and GABAergic neurons (67–69). Immunohistochemistry revealed a faint ZnT-3 signal in the IPL of intact mice. However, by 1 d after NC, the ZnT-3 signal had increased 2.8 ± 0.2-fold (mean ± SEM, Bonferroni-corrected $P < 0.0001$) and displayed a laminar distribution resembling that of $Zn^{2+}$ itself (Fig. 2 *A* and *B*; compare with. Fig. 1 *A–C*). At 3 d after NC,

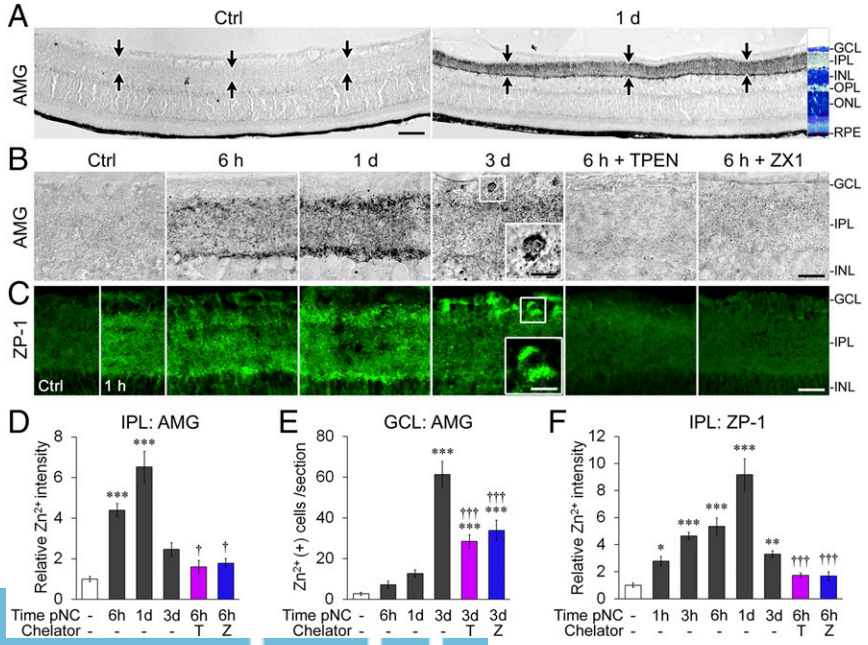


**Fig. 1.** Optic nerve injury leads to rapid elevation of $Zn^{2+}$ in the retina. (*A*) Low-magnification images of mouse retinas stained by $Zn^{2+}$-selenite AMG from an untreated control mouse (Ctrl, PBS-injected) and 1 d post-NC (pNC). Toluidine blue-stained section at right shows retinal layers. Areas between black arrows show the IPL. (Scale bar, 50 μm.) This panel shows composites of multiple images taken at the same exposure and magnification spliced together. (*B* and *C*) $Zn^{2+}$ accumulation visualized in retinal cross-sections by AMG (*B*) or the fluorescent $Zn^{2+}$ sensor ZP-1 (*C*). (Scale bars, 25 μm.) Boxed areas: Cellular staining in the GCL. (Scale bar, 10 μm.) Signals are eliminated by the $Zn^{2+}$ chelators TPEN and ZX1. (*D–F*) Quantitation of AMG staining in the IPL (*D*, $n = 12, 9, 14, 9, 6, 6$ retinas per group), positively stained cells in the GCL (*E*, $n = 6, 6, 8, 9, 6, 6$ retinas per group), and ZP-1 signal in the IPL (*F*, $n = 7, 7, 5, 6, 7, 5, 6, 6$ retinas per group). One-way ANOVA with Bonferroni post hoc tests. $^{*}P < 0.05$, $^{**}P < 0.01$, $^{***}P < 0.001$ compared with uncrushed controls; $^{\dagger}P < 0.05$, $^{\dagger\dagger\dagger}P < 0.001$ compared with 6h pNC. INL, inner nuclear layer; ONL, outer nuclear layer; OPL, outer plexiform layer; RPE, retinal pigment epithelium; T, TPEN; Z, ZX1.

ZnT-3 expression was elevated 1.8-fold in cells of the GCL, most of which are RGCs (Fig. S3 *C* and *D*). Introducing TPEN immediately after nerve injury suppressed the elevation of ZnT-3 (Bonferroni-corrected $P < 0.0001$) (Fig. 2 *A* and *B*), indicating that expression of the transporter protein is regulated by $Zn^{2+}$ concentration. ZnT-3 expression was not elevated in the eye contralateral to the NC (Fig. S3*A*), nor was it elevated in either eye by intravitreal injection of exogenous $Zn^{2+}$ ($ZnCl_2$, 100 μM, 1 mM) (Fig. S3*B*). To investigate the role of ZnT-3 in $Zn^{2+}$ accumulation, we used mice carrying a deletion of *slc30a3*, the gene encoding ZnT-3, along with wild-type littermates. *slc30a3* deletion eliminated the ZnT-3 signal in the retina ($P < 0.0001$, *t* test) (Fig. 2 *A* and *C*), verifying the validity of the immunostaining. Importantly, *slc30a3* deletion eliminated the $Zn^{2+}$ signal in the IPL 1 d after NC ($P = 0.0008$, *t* test) (Fig. 2 *D* and *E*) and eliminated ∼two-thirds of the cellular $Zn^{2+}$ staining in the GCL at 3 d ($P < 0.0001$, *t* test) (Fig. 2*F*). Thus, ZnT-3 increases in response to elevated $Zn^{2+}$, enables $Zn^{2+}$ to be sequestered in synaptic vesicles of the IPL, and is required for most, although not all, of the delayed $Zn^{2+}$ accumulation in cells of the GCL (shown below to be RGCs).

The loss of $Zn^{2+}$ accumulation in cells of the GCL following *slc30a3* deletion suggests that cellular accumulation may result from vesicular release of $Zn^{2+}$ from the processes of interneurons in the IPL. To test this idea, we injected tetanus neurotoxin (TeNT; 20 nM), an inhibitor of vesicular transmitter release, into the eye immediately after NC. TeNT blocked the decline in $Zn^{2+}$ that normally occurs in the IPL 3 d after NC, causing $Zn^{2+}$ levels in the IPL to increase 6.6 ± 0.4-fold ($P < 0.001$) over those seen in PBS-treated retinas after NC (16.3 ± 1.0-fold increase compare with normal retina) (Fig. 2 *G* and *I*). Concurrently, TeNT caused the number of $AMG^+$ cells in the GCL to decline by ∼two-thirds relative to the number seen in PBS-injected controls (Fig. 2 *G* and *H*). Deletion of *slc30a3* suppressed the effects of TeNT on $Zn^{2+}$ accumulation in the IPL, confirming that $Zn^{2+}$ accumulation reflects presynaptic vesicular $Zn^{2+}$ (Fig. 2 *G* and *I*). Even in the absence of NC, TeNT caused an 11.4 ± 0.8-fold increase in $Zn^{2+}$ accumulation in the IPL compared with the normal retina ($P < 0.001$). This finding suggests that vesicular release of $Zn^{2+}$ may occur in the normal IPL.

**Cellular Localization of ZnT-3 and $Zn^{2+}$.** The stratified, punctate distribution of ZnT-3 and $Zn^{2+}$ in the IPL resembles the laminar distribution of synapses that arise from particular classes of interneurons (70), raising the question of cell-type specificity. Double-immunostaining and confocal microscopy revealed a strong overlap between ZnT-3 and two markers for amacrine cell synapses, the vesicular GABA transporter VGAT (85 ± 2.3% overlap, mean ± SEM) and glutamic acid decarboxylase (GAD)-65/-67 (73.3 ± 4.0% overlap) (Fig. 3 *A* and *D* and Fig. S3 *E* and *G*). Conversely, ZnT-3 showed only a small overlap with two markers for bipolar cell synapses, vesicular glutamate transporter-1 (VGLUT1, 7.1% overlap, Bonferroni-corrected $P < 0.0001$) (Fig. 3 *B* and *D* and Fig. S3*G*) and protein kinase C-α (PKCα, 6.4% overlap, Bonferroni-corrected $P < 0.0001$) (Fig. S3 *F* and *G*). ZnT-3 is also reported to be expressed in Müller cells (71, 72), and we therefore carried out colocalization studies for ZnT-3 and the Müller cell marker, cellular retinaldehyde binding protein (CRALBP). The overlap was found to be 2.8% (Fig. 3 *C* and *D* and Fig. S3*G*). We were unable to localize the $Zn^{2+}$ signal itself by double-labeling because of the incompatibility of

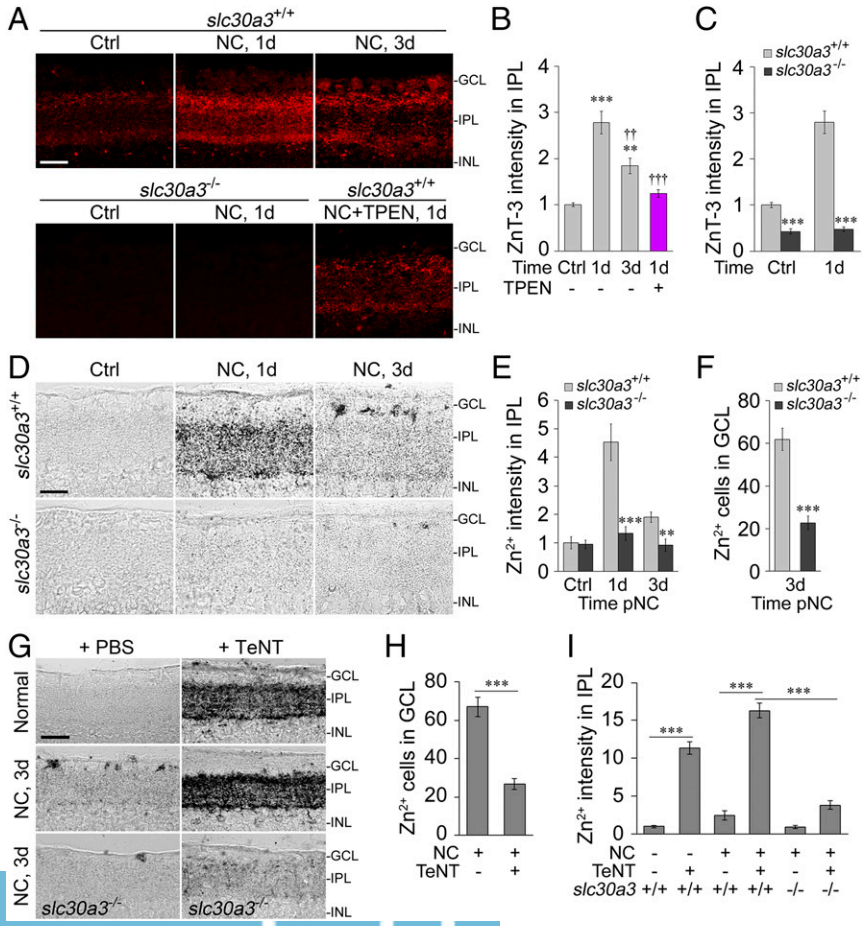


**Fig. 2.** $Zn^{2+}$ accumulation in the IPL and subsequent transfer to cells of the GCL: role of ZnT-3. (*A*) ZnT-3 immunostaining in retinas of *slc30a3*$^{+/+}$ and *slc30a3*$^{-/-}$ littermates. (Scale bar, 25 μm.) (*B*) Quantitation of ZnT-3 immunostaining in the IPL before and after NC in wild-type mice with and without TPEN treatment (normalized to normal control; $n = 10, 8, 8, 6$). One-way ANOVA, $^{**}P < 0.01$, $^{***}P < 0.001$ respectively compared with uncrushed controls; $^{††}P < 0.01$, $^{†††}P < 0.001$ compared with 1d pNC. (*C*) Quantitation of ZnT-3 expression in IPL of *slc30a3*$^{-/-}$ retinas and *slc30a3*$^{+/+}$ littermates (normalized; $n = 10, 8; 8, 6$ retinas per group). Unpaired *t* test, $^{***}P < 0.001$ compared with *slc30a3*$^{+/+}$ littermate controls. (*D–F*) Images (*D*) and quantitation of AMG staining in IPL (*E*, $n = 6$ retinas per group) and GCL (*F*, cells per 14-μm section; $n = 6$ retinas per group) of *slc30a3*$^{-/-}$ and *slc30a3*$^{+/+}$ littermates. Unpaired *t* test. $^{**}P < 0.01$, $^{***}P < 0.001$ compared with *slc30a3*$^{+/+}$ littermate controls. (Scale bar, 25 μm.) (*G–I*) TeNT blocks vesicular release of $Zn^{2+}$, causing continued $Zn^{2+}$ build-up in the IPL and diminished accumulation in cells of the GCL. (*G*) Images show AMG staining 3 d after intraocular injection of TeNT (20 nM). Note reduced number of $Zn^{2+}$-positive cells in the GCL. Deletion of *slc30a3*, the gene encoding ZnT-3, eliminates $Zn^{2+}$ accumulation in IPL. (Scale bar, 50 μm.) (*H* and *I*) Quantitation of $Zn^{2+}$-positive cells in the GCL (*H*, cells per 14-μm section) and intensity in the IPL (*I*, normalized). $n = 6, 7$ in *H* and $n = 12, 4, 6, 7, 6, 6$ in *I*. Unpaired *t* test, $^{***}P < 0.001$, comparison between indicated groups. All data represent mean ± SEM.

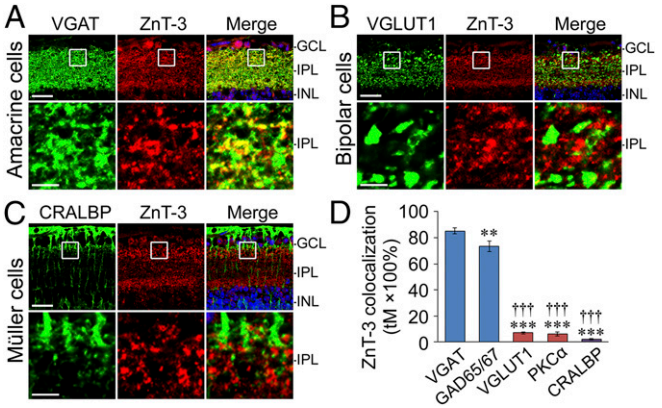


**Fig. 3.** ZnT-3 is localized in amacrine cell processes. (*A–C*) Confocal images through retinal cross-sections show a strong overlap of ZnT-3 with the amacrine cell marker VGAT (*A*), but much less overlap with the bipolar cell marker VGLUT1 (*B*) or the Müller cell marker CRALBP (*C*). [Scale bars, 25 μm (lower-magnification), 5 μm (higher-magnification).] (*D*) Colocalization frequency (Mander's value, tM) of ZnT-3 with cell type-specific markers (see also Fig. S3 *E–G*). $n = 10$ retinas per group, one-way ANOVA with Bonferroni post hoc tests. $^{**}P < 0.01$, $^{***}P < 0.001$ compare with VGAT; $^{\dagger\dagger\dagger}P < 0.001$ compare with GAD65/67. All bars show mean ± SEM.

immunostaining with either AMG (which forms an electron-dense reaction product and requires glutaraldehyde fixation, thereby suppressing antigenicity and causing high autofluorescence) or with ZP-1, because of a rapid loss of the fluorescent signal during the course of immunostaining. We therefore used adeno-associated viruses (AAVs) that preferentially infect different cell types to express the fluorescent protein mCherry primarily in either RGCs (AAV2) or interneurons (AAV6) (73, 74). As expected from the double-immunostaining results for ZnT-3, at 24 h after NC the ZP-1 signal partially overlapped with mCherry encoded by AAV6 (Fig. S4*A*), which in turn overlapped with the amacrine cell markers VGAT (Fig. S4*B*) and GAD-65/67 (Fig. S4*C*). The ZP-1 signal at 24 h after NC did not overlap with the bipolar cell markers VGLUT1 or PKCα (Fig. S4 *E* and *F*) nor with βIII-tubulin, which in the retina is only expressed in RGCs (75) (Fig. S4*D*). At 3 d, however, the ZP-1 signal overlapped with mCherry expressed by AAV2 (Fig. S4*G*), which in turn colocalized with the RGC marker βIII-tubulin (Fig. S4*H*). These findings indicate that $Zn^{2+}$ first accumulates primarily in ZnT-3–containing vesicles in amacrine cells and subsequently appears within RGCs. AMG staining revealed the presence of some $Zn^{2+}$ within the optic nerve, but this signal was only mildly altered by NC and was unaffected by intraocular injection of chelators (Fig. S5 *A* and *B*). Mice lacking ZnT-3 had somewhat lower $Zn^{2+}$ levels in the optic nerve than *slc30a3*$^{+/+}$ littermates (Fig. S5 *C* and *D*).

**Elimination of Vesicular $Zn^{2+}$ Promotes RGC Survival and Axon Regeneration.** To determine the consequences of $Zn^{2+}$ elevation in amacrine cell processes, we examined whether elimination of ZnT-3 would alter RGC survival and axon regeneration after NC. Mice lacking *slc30a3* showed twice the number of RGCs surviving 2 wk after NC as *slc30a3*$^{+/+}$ littermates (unpaired *t* test, $P < 0.0001$) (Fig. 4 *A* and *B*) and nearly 10 times the level of axon regeneration (unpaired *t* test, $P < 0.0001$) (Fig. 4 *C* and *D*). It is important to note that, because *slc30a3* deletion does not fully eliminate $Zn^{2+}$ accumulation in RGCs (Fig. 2*F*), the effects of gene deletion on cell survival and axon regeneration may not fully represent the effects of removing $Zn^{2+}$ from the system. Two weeks after NC, the survival of RGCs in wild-type (*slc30a3*$^{+/+}$) littermates of *slc30a3*$^{-/-}$ mice (23.8%) was somewhat greater than that of C57 mice (16.3%) (Fig. 5*G*). The likely basis for this difference is that the *slc30a3*$^{-/-}$ mice were generated on a mixed 129S/C57 background, and pure 129S mice have a 2-wk survival rate of ∼26.1% (Fig. S6*D*). Finally, as an additional test of whether vesicular $Zn^{2+}$ is the pool responsible for RGC death, we investigated RGC survival 2 wk after intraocular injection of TeNT. TeNT increased RGC survival more than twofold (39.1%) (Fig. S6 *G* and *H*), similar to the effect seen after *slc30a3* deletion (Fig. 4*B*).

**Intraocular $Zn^{2+}$ Chelation Attenuates RGC Death.** To investigate whether the effects of suppressing $Zn^{2+}$ elevation in the retina can be achieved pharmacologically, we examined whether $Zn^{2+}$ chelators could affect RGC survival when administered after NC. Intraocular injection of TPEN or ZX1 (100 μM) immediately after NC and 4 d later nearly doubled overall RGC survival compared with controls receiving PBS injections (both Bonferroni-corrected $P < 0.0001$) (Fig. 5 *A–D* and *G*; dose–response data in Fig. S6 *A* and *B*). The effects of the chelators on cell survival were independent of the distance of RGCs from the center of the retina (Fig. S6*C*). The survival effects of the chelators were suppressed when saturated with equimolar $Zn^{2+}$ (Bonferroni-corrected $P_{TPEN} = 0.011$, $P_{ZX1} = 0.0008$) (Fig. 5 *E–G*). Because $Zn^{2+}$ increases so rapidly after NC, we tested whether having chelators present at the time of NC would have an even stronger benefit. However, an additional injection of either chelator 1 d before NC did not increase RGC survival above the level achieved by postinjury treatment (Fig. 5*G* and Fig. S6*E*). We also investigated whether $Zn^{2+}$ elevation lies upstream of other changes known to occur in RGCs after NC. TPEN and ZX1 suppressed the injury-induced elevation of active caspase-3 and the loss of Bcl-xL that occur after NC (76, 77) (all Bonferroni-corrected $P < 0.01$) (Fig. 5 *I* and *J* and Fig. S6 *I* and *J*). TPEN also suppressed the elevation of CCAAT-enhancer binding protein homologous protein (CHOP) (4) (Bonferroni-corrected $P = 0.0029$) (Fig. S7), whereas ZX1 had a somewhat lesser effect, although in the same direction (not significant). Combining *slc30a3* deletion with TPEN did not augment 2-wk survival beyond the level achieved with either one alone (Fig. 5*H*) (Bonferroni-corrected $P > 0.999$).

**Combinatorial Therapy and Enduring RGC Survival.** In the absence of any interventions, RGCs continue to die after NC and only ∼2%

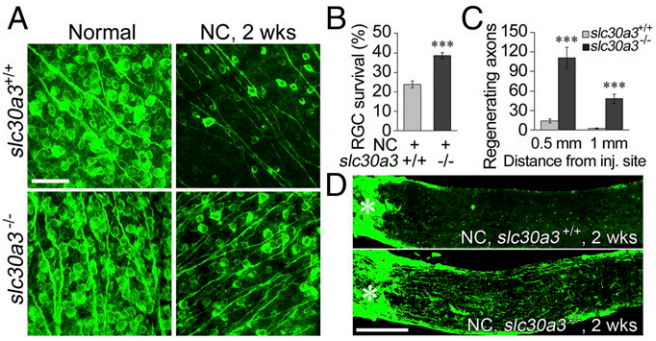


**Fig. 4.** Elimination of the vesicular $Zn^{2+}$ transporter ZnT-3 promotes RGC survival and axon regeneration. (*A* and *B*) RGC survival. (*A*) Retinal whole-mounts immunostained for βIII-tubulin to visualize RGCs in retinas of normal control mice or in mice 2 wk pNC, with or without deletion of *slc30a3*, the gene for ZnT-3. No general abnormalities were observed in the retinas of mice lacking *slc30a3* (with or without NC). (Scale bar, 50 μm.) (*B*) Effect of *slc30a3* deletion on RGC survival: quantitation. $n = 8, 10$; unpaired *t* test, $^{***}P < 0.001$ compared with *slc30a3*$^{+/+}$ controls. (*C* and *D*) Quantitation (*C*) and images (*D*, GAP-43 immunostaining) showing effects of *slc30a3* deletion on optic nerve regeneration 2 wk pNC. $n = 8, 10$; unpaired *t* test, $^{***}P < 0.001$ compared with *slc30a3*$^{+/+}$ controls. (Scale bar, 200 μm.) Asterisks denote injury site. *D* shows composites of multiple images taken at the same exposure and magnification spliced together.

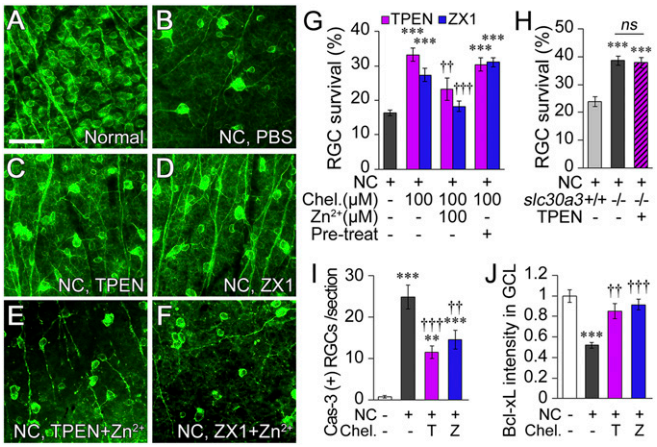


**Fig. 5.** Chelating $Zn^{2+}$ enhances RGC survival. (*A–F*) Retinal whole-mounts immunostained for βIII-tubulin to visualize RGCs in normal control mice (*A*) or 2 wk pNC with treatments as indicated. (Scale bar, 50 μm.) (*G*) Quantitative results. [Chel, chelators; Pretreat, additional injection given 1 d before NC; $n$ = 11, 6, 6, 6 (TPEN); $n$ = 11, 7, 8, 6 (ZX1)]. One-way ANOVA, Bonferroni post hoc tests. $^{***}P < 0.001$ compared with NC alone; $^{\dagger\dagger}P < 0.01$, $^{\dagger\dagger\dagger}P < 0.001$ for decrease compared with chelator-alone group. (*H*) Combined effects of TPEN treatment and *slc30a3* deletion. $n$ = 8, 10, 10; one-way ANOVA with Bonferroni post hoc tests, $^{***}P < 0.001$ compared with *slc30a3*$^{+/+}$ controls. (*I* and *J*) Chelator effects on cleaved caspase-3 and the antiapoptotic protein Bcl-xL 5 d after NC (images are in Fig. S6 *I* and *J*). Values in *J* are normalized to uncrushed controls. $n$ = 6 per group, one-way ANOVA with Bonferroni post hoc tests. $^{**}P < 0.01$, $^{***}P < 0.001$ compared with uncrushed controls; $^{\dagger\dagger}P < 0.01$, $^{\dagger\dagger\dagger}P < 0.001$ compared with NC-alone group. All bars show mean ± SEM.

remain alive after 12 wk (two-way ANOVA, Bonferroni-corrected $P$ = 0.0006) (Fig. 6). In marked contrast, the effects of $Zn^{2+}$ chelation on RGC survival endured, with the number of viable RGCs remaining nearly constant for 12 wk (two-way ANOVA, Bonferroni-corrected $P > 0.99$, comparing survival at 12 wk vs. 2 wk). Even more striking effects were seen when TPEN was combined with deletion of phosphatase and tensin homolog (*pten*), a suppressor of the PI3 kinase-Akt pathway. Although *pten* deletion has been shown to promote RGC survival and axon regeneration after optic nerve injury (13) (Fig. 6), this effect declined sharply over time, with only ~12% of RGCs remaining alive at 12 wk (two-way ANOVA, Bonferroni-corrected $P < 0.0001$, survival at 12 wk vs. 2 wk) (Fig. 6). Combining TPEN and deletion of *pten* (via AAV2-Cre–induced *pten* deletion in *pten*$^{flx/flx}$ mice) stabilized the high level of neuroprotection afforded by *pten* deletion, enabling nearly half of all RGCs to survive at least 3 mo after NC (two-way ANOVA, Bonferroni-corrected $P$ = 0.92 comparing survival at 12 wk vs. 2 wk) (Fig. 6). Thus, early blockade of $Zn^{2+}$ elevation provides long-term protection for many RGCs and stabilizes the high but otherwise transient neuroprotective effect of *pten* deletion. *slc30a3* deletion also maintained high levels of RGC survival over a period of months, although to a somewhat lesser extent than TPEN (Fig. S6 *L* and *M*).

**$Zn^{2+}$ Chelation Promotes Axon Regeneration.** We next investigated whether $Zn^{2+}$ influences RGCs' ability to regenerate axons. For this, we used GAP-43 immunostaining to quantify the number of axons extending selected distances beyond the injury site 2 wk after NC in the presence or absence of chelators (78). Whereas untreated controls showed only a handful of axons beyond the injury site 2 wk after NC and PBS injection (7.0 ± 2.5, mean ± SEM) (Fig. 7*A*), mice receiving intraocular TPEN or ZX1 (100 μM) immediately after NC and 4 d later showed a 25-fold increase in regeneration (180.7 ± 30.2 axons for TPEN, 164.4 ± 31.3 for ZX1: Bonferroni-corrected $P_{TPEN}$ = 0.0002, $P_{ZX1}$ = 0.0029) (Fig. 7*B* and Fig. S8 *A–C*). To verify that the observed differences in axons counted in the nerve were not a result of changes in GAP-43 expression or to a differential survival of axons after injury, we generated a separate cohort of mice to compare the numbers of axons distal to the injury site by GAP-43 immunostaining vs. anterograde tracing with cholera toxin B fragment (CTB, injected intraocularly 4 d before tissue harvest). The two methods gave nearly identical results (Fig. S9*C*) when analyzed by either anatomical colocalization (Fig. S9 *A* and *B*) or by quantitation of each label separately (Fig. S9*D*). The effects of TPEN and ZX1 were nearly eliminated by presaturating chelators with equimolar $Zn^{2+}$ (Bonferroni-corrected $P_{TPEN}$ = 0.013, $P_{ZX1}$ = 0.039) (Fig. 7*B* and Fig. S8 *A–C*), demonstrating the specificity of these effects to $Zn^{2+}$. As with cell survival, we also examined the effect of introducing chelators before the time of NC. Whereas pretreatment did not augment RGC survival, introducing an additional injection of TPEN or ZX1 before nerve injury doubled the amount of regeneration compared with that seen when chelators were only introduced afterward (Bonferroni-corrected $P_{TPEN}$ = 0.0033, $P_{ZX1}$ = 0.013) (Fig. 7 *A* and *B* and Fig. S8 *B* and *C*). Combining ZnT-3 deletion with TPEN-mediated $Zn^{2+}$ chelation immediately after NC and 4-d later resulted in a level of regeneration similar to that of either treatment alone (Bonferroni-corrected $P > 0.99$) (Fig. 7*E*; compare with Fig. 7*B*).

**Combinatorial Therapy.** The level of regeneration seen after introducing chelators before and after NC is comparable to that obtained by preinjury deletion of *pten* or by intraocular injections of Zymosan with a cAMP analog, two of the strongest treatments reported to date (13, 19). As noted above, *pten* deletion in RGCs was achieved by intraocular injection of an AAV-expressing Cre recombinase (AAV2-Cre) in *pten*$^{flx/flx}$ mice 2 wk before NC. Combining $Zn^{2+}$ chelation with *pten* deletion had a much greater effect than either treatment alone, and enabled some axons to extend to the far end of the optic nerve in just 2 wk (all Bonferroni-corrected $P < 0.05$) (Fig. 7 *C* and *D*, and Fig. S8*D*). By 12 wk, the number of axons growing the full length of the nerve continued to increase and many crossed the optic chiasm (all Bonferroni-corrected $P < 0.05$) (Fig. 7 *F–H*). TPEN did not, however, augment regeneration induced by Zymosan/CPT-cAMP (Fig. 7*D*).

To examine the effects of $Zn^{2+}$ chelation on gene transcription, we used a panel of probes similar to those recently used to investigate the role of dual-leucine kinase (DLK) following NC (2). TPEN increased the expression of multiple genes associated with axon regeneration, including *gap43*, *sprr1a*, *fn14*, *atf3*, and *Klf6* (all Bonferroni-corrected $P < 0.05$) (Fig. S7). ZX1 had

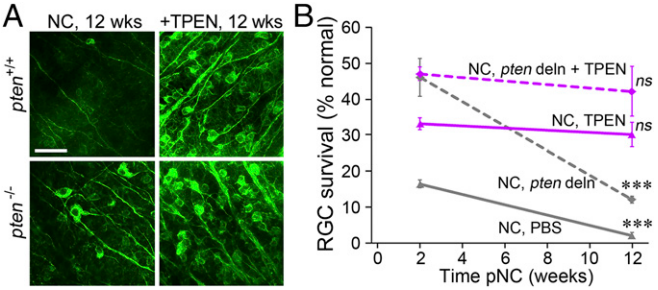


**Fig. 6.** $Zn^{2+}$ chelation leads to long-term RGC survival and stabilizes the effects of *pten* deletion. (*A*) Portions of flat-mounted retinas immunostained for βIII-tubulin to visualize surviving RGCs 12 wk after NC with and without TPEN treatment or *pten* deletion. (Scale bar, 50 μm.) (*B*) Quantitation of long-term RGC survival. $n$ = 11, 6, 6, 10 (2 wk); $n$ = 9, 6, 6, 6 (12 wk), two-way ANOVA with Bonferroni post hoc tests; $^{***}P < 0.001$ compared with the same treatment at 2 wk after NC; *ns*, not significant. All data points represent mean ± SEM.

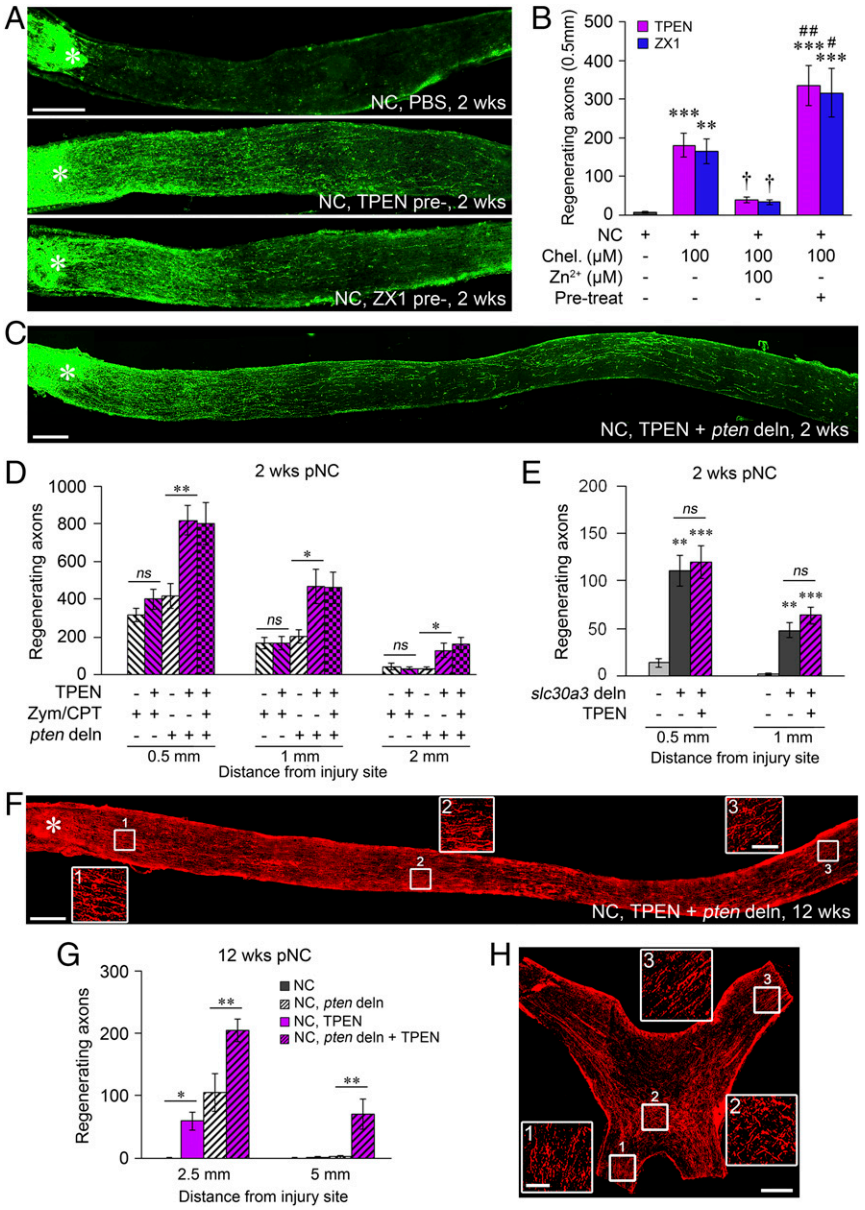


**Fig. 7.** $Zn^{2+}$ chelation promotes optic nerve regeneration. (*A* and *B*) Longitudinal sections through the mouse optic nerve immunostained for GAP-43 2 wk pNC (*A*) and quantification of results (*B*) (asterisk: injury site) (Scale bar, 200 μm.) (Chel, chelators; Pretreat, additional injection given one day before NC in *B*). $n$ = 10, 8, 7, 6 (TPEN) and 10, 7, 6, 6 (ZX1). One-way ANOVA, Bonferroni post hoc tests. $^{**}P < 0.01$, $^{***}P < 0.001$ compared with NC alone; $^{\dagger}P < 0.05$, decrease compared with chelator-alone group; $^{\#}P < 0.05$, $^{\#\#}P < 0.01$, increases compared with chelator-alone group. (*C* and *D*) Image (*C*) and quantitation (*D*, $n = 6$ per group) showing axon regeneration in mice with intraocular TPEN combined with *pten* deletion in RGCs. One-way ANOVA with Bonferroni post hoc tests. (Scale bar, 200 μm.) $^{*}P < 0.05$, $^{**}P < 0.01$; *ns*, not significant. (*E*) Quantitation showing effects of *slc30a3* deletion, with and without TPEN treatment, on optic nerve regeneration 2 wk pNC. $n$ = 8, 10, 18; one-way ANOVA with Bonferroni post hoc tests, $^{**}P < 0.01$, $^{***}P < 0.001$ compared with *slc30a3*$^{+/+}$ controls. (*F–H*) Image (*F*) and quantitation (*G*) showing regeneration induced by combining TPEN and *pten* deletion 12 wk pNC. *G*, ($n$ = 8, 5, 5, 6). One-way ANOVA with Bonferroni post hoc tests. $^{*}P < 0.05$, $^{**}P < 0.01$. *F* and *H*, CTB-labeled axons in the optic nerve (*F*, single 14-μm section) and optic chiasm (*H*, stack of three 14-μm sections). (Scale bars, 200 μm in main images, 50 μm in enlarged areas.) All bars show mean ± SEM. *A*, *C*, *F*, and *H* represent composites of multiple images taken at same exposure conditions spliced together.

qualitatively similar effects, although in some cases these did not achieve statistical significance (Fig. S7).

**Therapeutic Window.** Because treatment in a clinical setting might be delayed for hours or days, we investigated the efficacy of beginning $Zn^{2+}$ chelation well after injury had occurred. TPEN had equally strong effects on RGC survival whether administered immediately after injury or 1 d later (Fig. 8*A*) (both Bonferroni-corrected $P < 0.0001$ compared with untreated control) and was only slightly less effective when applied after a 5-d delay (Fig. 8*A*) (Bonferroni-corrected $P < 0.0001$ compared with untreated control, $P = 0.2762$ compared with D0). Our standard treatment regimen, injecting TPEN immediately after injury and again 4 d later, was more effective than a single early injection (Fig. 8*B*) (unpaired $t$ test, $P = 0.02$ compared with D0 only), and the addition of a third injection on day 7 increased RGC survival to nearly 40% (Fig. 8*B* and Fig. S6*F*) (unpaired $t$ test, $P = 0.0052$ compared with two treatments at D0 and D4).

The benefit of $Zn^{2+}$ chelation on axon regeneration followed a different pattern from that seen for cell survival. A single injection of TPEN (100 μM) stimulated regeneration even if delayed for 5 d (Fig. 8*C*) (all Bonferroni-corrected $P < 0.05$). However, treatment at 5 d resulted in approximately half the level of regeneration observed when TPEN was introduced immediately after nerve injury. The standard treatment regimen used in our study, one injection shortly after injury and a second one 4-d later, was about twice as effective as a single early postinjury injection (unpaired $t$ test, $P = 0.033$) (Fig. 8 *C* and *D*), although the inclusion of a third injection on day 7 had no further benefit. The relative benefits of early treatment are consistent with the dramatic regeneration seen when chelators were present before optic nerve injury (Fig. 7*B*).

Taken together, these results indicate that the $Zn^{2+}$-dependent processes that suppress RGC survival and axon regeneration persist for several days after optic nerve injury, affording an appreciable therapeutic window, and that repeated treatments further augment survival and regeneration.

## Discussion

Recovery after CNS injury is restricted in part by the inability of mature neurons to regenerate axons over long distances, the limited capacity of neurons to form compensatory circuits, and in

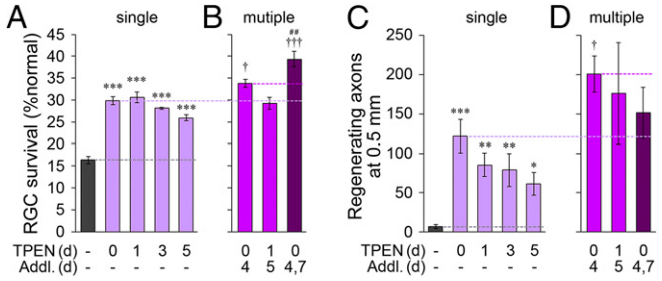


**Fig. 8.** Therapeutic window for $Zn^{2+}$ chelation. (*A* and *B*) Surviving RGCs following the same treatments described above. (*A*) Single treatments, $n$ = 11, 6, 20, 6, 21; (*B*) multiple treatments, $n$ = 15, 19, 8 retinas per group. (*C* and *D*) Number of regenerating axons 0.5 mm from the injury site 2 wk after TPEN treatment (100 μM) at the indicated time points (days, d) after NC. (*C*) Single injections, $n$ = 10, 8, 10, 8, 11 cases per group. (*D*) Multiple injections, $n$ = 14, 10, 8 cases per group. Addl, additional TPEN injection. One-way ANOVA with Bonferroni post hoc tests. $^{*}P < 0.05$, $^{**}P < 0.01$, $^{***}P < 0.001$ compared with PBS-treated controls; unpaired $t$ test, $^{\dagger}P < 0.05$, $^{\dagger\dagger\dagger}P < 0.001$ compared with single TPEN treatment; unpaired $t$ test, $^{\#\#}P < 0.01$ compared with TPEN treatments on days 0 and 4. All bars represent mean ± SEM.

the case of optic nerve damage, the death of RGCs. Although RGC death and regenerative failure have been widely attributed to cell-intrinsic processes, the glial environment, and an insufficiency of trophic agents, addressing these factors has thus far resulted in transient RGC survival, limited regeneration, or persistent RGC survival in a compromised state (79–82). Our results show that both RGC death and regenerative failure are caused in part by $Zn^{2+}$ dyshomeostasis, and that chelating $Zn^{2+}$ enables many injured RGCs to survive for months and regenerate axons, with a therapeutic window that persists for several days after injury.

The vast majority (~90%) of total zinc in neurons is tightly bound in metalloenzymes, transcription factors, and other zinc-containing proteins, in which zinc serves as a cofactor for enzymatic activity or maintaining the three-dimensional structure of proteins (83, 84). The remaining 10% of total zinc is referred to as chelatable, free, or mobile zinc, and is present as hydrated ions or is loosely bound to protein. These chelatable $Zn^{2+}$ ions, which in neurons are localized primarily in synaptic vesicles of so-called zinc-enriched neurons, can be detected by either fluorescence or AMG techniques. Although AMG detects copper (85) and iron (86), as well as zinc (62, 87, 88), ZP1 is highly selective for $Zn^{2+}$ and its intrinsic fluorescence is quenched by copper, iron, manganese, and cobalt ions (38, 66, 89). Thus, the fact that we observed similar changes in $Zn^{2+}$ with AMG and ZP1 reinforces the conclusion that elevation of $Zn^{2+}$ itself is occurring after NC. However, the question remains as to whether the functional effects of TPEN and ZX1 are a result of chelating $Zn^{2+}$ rather than another divalent cation. $Ca^{2+}$ can be ruled out because it does not interact with ZX1 (38, 66), which has the same effects as TPEN on survival and regeneration following optic nerve injury. The observation that the functional effects of TPEN are abrogated when it is presaturated with $Zn^{2}$ argues against involvement of biologically relevant divalent cations that bind the chelators with a higher affinity than $Zn^{2+}$ ($K_d = 2.6 \times 10^{-16}$ M), including $Cu^{2+}$ ($K_d = 3 \times 10^{-20}$ M), although not, strictly speaking, of cations that bind TPEN with a lower affinity than $Zn^{2+}$ (e.g., $Fe^{2+}$, $K_d = 2.4 \times 10^{-15}$ M; $Mn^{2+}$, $K_d = 5.4 \times 10^{-11}$ M; $Ca^{2+}$, $K_d = 4 \times 10^{-5}$ M; $Mg^{2+}$, $K_d = 2 \times 10^{-2}$ M) (90–92). However, several other lines of evidence point to the relevant ion being $Zn^{2+}$. First, the effects of the chelators in promoting RGC survival and axon regeneration closely match their ability to remove $Zn^{2+}$ per se, as visualized by the staining. Second, deletion of the $Zn^{2+}$ transporter ZnT-3 (68, 93, 94) similarly renders $Zn^{2+}$ undetectable in the IPL (Fig. 2 *D* and *E*) and has the same functional effects as the chelators (Fig. 4). Similarly, blocking vesicular release with TeNT suppresses the transfer of $Zn^{2+}$ to RGCs and attenuates RGC death.

The IPL, the initial site of $Zn^{2+}$ accumulation, contains distinct sublayers in which diverse types of interneurons synapse onto the dendrites of particular RGC subtypes or other interneurons in a stereotyped manner (70). RGCs receive excitatory inputs from bipolar cells that use glutamate as a transmitter and inhibitory inputs from amacrine cells that use either glycine or GABA as a transmitter. Many interneurons also contain peptides or monoamine neurotransmitters (95, 96). Like $Zn^{2+}$ localization in other parts of the CNS (93), $Zn^{2+}$ accumulation in the IPL was found to require ZnT-3, as evidenced by the loss of detectable $Zn^{2+}$ when *slc30a3* was deleted. Reciprocally, increased ZnT-3 expression required elevation of free $Zn^{2+}$, implying that ZnT-3 expression depends on $Zn^{2+}$ concentration and that $Zn^{2+}$ sequestration in turn relies on ZnT-3 levels. The loss of detectable $Zn^{2+}$ after NC when ZnT-3 was deleted is consistent with prior work showing that AMG preferentially detects $Zn^{2+}$ that is present at high concentrations within vesicles (93). However, the absence of an AMG signal does not imply that $Zn^{2+}$ is not being liberated by upstream signals (see below) or that it might not still be present in other cellular compartments at lower concentrations. It is also possible that the failure to detect $Zn^{2+}$ in the absence of ZnT-3 is because vesicular sequestration acts as a sink for $Zn^{2+}$, without which other transporters and homeostatic mechanisms prevent the accumulation of high levels of cytoplasmic $Zn^{2+}$. Within the first day after NC, $Zn^{2+}$ and ZnT-3 were localized primarily in amacrine cell processes, whereas at 3 d, $Zn^{2+}$ was found mostly in RGCs. Elsewhere in the CNS, although most $Zn^{2+}$-containing synapses are glutamatergic (47, 97), prior studies have reported the presence of $Zn^{2+}$ in amacrine cells (42) and in inhibitory synapses of the brainstem (98).

Along with suppressing vesicular $Zn^{2+}$ accumulation in the IPL, deletion of *slc30a3* suppressed the subsequent signal in RGCs, as did the chelators. These observations, together with our finding that TeNT causes $Zn^{2+}$ to continue building up in the IPL while decreasing $Zn^{2+}$ accumulation in RGCs, point to the transfer of $Zn^{2+}$ from synaptic vesicles in amacrine cell processes as the primary source of $Zn^{2+}$ elevation in RGCs. Importantly, the functional consequences of *slc30a3* deletion and $Zn^{2+}$ chelation were non-additive, implying that the negative effects of $Zn^{2+}$ on both RGC survival and axon regeneration are associated primarily with its initial vesicular sequestration in amacrine cells. It is important to note, however, that even with *slc30a3* deletion, $Zn^{2+}$ chelation, or intraocular TeNT, many RGCs go on to die within the first 2 wk. This result may be a consequence of the continued low-level accumulation of $Zn^{2+}$ in RGCs that we observed after early chelator application (Fig. 5 and Fig. S1*F*) and even after preventing vesicular sequestration by *slc30a3* deletion (Figs. 2*F* and 4) or after blocking vesicular release (with TeNT) (Fig. 2 *G–I* and Fig. S6 *G* and *H*). Continued low-level release of zinc has also been demonstrated after ZnT-3 deletion in the auditory brainstem (40), suggesting the presence of nonvesicular $Zn^{2+}$ release. In addition, it is possible that RGCs possess both $Zn^{2+}$-dependent and $Zn^{2+}$-independent pathways for cell death, or that some $Zn^{2+}$ accumulation may occur in RGCs via cell-autonomous mechanisms (58, 59). Finally, because $Zn^{2+}$ has beneficial effects, such as modulating synaptic transmission and BDNF synthesis, removing $Zn^{2+}$ could potentially have mixed positive and negative effects on RGCs (38, 40, 99, 100).

The rapid elevation of $Zn^{2+}$ in the IPL following optic nerve injury is concurrent with other early changes that occur in this system: that is, $Ca^{2+}$ elevation and activation of MAP kinase cascades that include DLK, c-jun N-terminal kinases (Jnk2 and -3), ASK-1 and P38, and c-Jun phosphorylation (2, 3, 7, 9, 10, 101). Blocking these latter changes results in substantial cell survival that diminishes over time and modest or no regeneration (2, 3, 7, 9, 10). Subsequent changes include down-regulation of IGF1 and phospho-Akt, increases in reactive oxygen species, the unfolded protein response and endoplasmic reticulum stress,

caspase activation, histone deacetylation, gene silencing, diminished intracellular cAMP, and changes in levels of anti- and proapoptotic Bcl-like proteins (4–6, 8). Although the mechanistic relationships between $Zn^{2+}$ dysregulation and these other changes remains to be investigated, the observations that $Zn^{2+}$ chelation diminishes several hallmarks of RGC death (caspase 3 activation, CHOP expression, Bcl-xL down-regulation), affords long-term survival for many RGCs, and stabilizes the high but transient neuroprotective effects of *pten* deletion (Fig. 6), indicate that $Zn^{2+}$ plays an early and critical role in regulating RGC death. In terms of cell-type specificity, *pten* deletion selectively enhances the survival of RGCs with high basal mammalian target of rapamycin (mTOR) activity (20), but only transiently (Fig. 6). The ability of TPEN to stabilize the survival of RGCs lacking *pten* suggests that $Zn^{2+}$ chelation may selectively stabilize the survival of the same types of RGCs that are protected by *pten* deletion, although further work is needed to confirm this point. In terms of upstream mechanisms, NO produced via NOS1 mobilizes $Zn^{2+}$ from metallothioneins (102, 103) in various neurological disorders (47, 59), and our preliminary studies indicate that NOS1-derived NO lies upstream of $Zn^{2+}$ elevation in amacrine cell processes (104).

The level of regeneration induced by introducing $Zn^{2+}$ chelators before and after NC is comparable to that obtained by other effective proregenerative treatments, such as deleting *pten* before nerve injury or injecting Zymosan plus a cAMP analog after injury. *pten* deletion de-represses PI3 kinase-Akt signaling (13) and promotes regeneration for only αRGCs (20). Combining $Zn^{2+}$ chelation with *pten* deletion enabled some axons to regenerate the full length of the optic nerve in just 2 wk, and by 12 wk many axons had crossed the optic chiasm. It will be important to determine whether this latter combination expands the types of RGCs that regenerate axons beyond αRGCs. Another method to promote regeneration is by inducing intraocular inflammation, for example, with Zymosan, which causes an infiltration of neutrophils and macrophages that secrete oncomodulin, an 11-kDa growth factor that stimulates outgrowth from RGCs in a cAMP-dependent manner (18, 19). Combining Zymosan/CPT-cAMP with *pten* deletion appears to expand the RGC subtypes that regenerate axons, as inferred by the multiple target areas of the brain that become reinnervated (27). However, $Zn^{2+}$ chelation did not enhance the effects of Zymosan, perhaps because the two treatments activate a common downstream pathway.

$Zn^{2+}$ chelation improved cell survival and axon regeneration even when treatment was delayed for several days, and repeated treatments were more effective than a single treatment. Thus, the $Zn^{2+}$-sensitive processes that suppress axon regeneration and cell survival appear to continue well beyond the time of nerve injury. However, whereas the benefits of chelation on cell survival were relatively constant over the first 5 d and were unaffected by pretreatment, chelation immediately after nerve injury resulted in twice the level of regeneration seen when treatment was delayed for 5 d, and pretreatment doubled the level of regeneration obtained by postinjury treatment alone. These results point to a considerable therapeutic window to improve RGC survival and augment the effects of other proregenerative treatments by using $Zn^{2+}$ chelators after optic nerve injury. However, the mechanisms underlying the differential effects of early chelation on regeneration vs. cell survival remains unknown.

In conclusion, we report that $Zn^{2+}$ accumulates rapidly in amacrine cell processes after the optic nerve is injured and that chelating $Zn^{2+}$ results in both enduring RGC survival and considerable axon regeneration. Our results also provide evidence for rapid retrograde signaling between axotomized RGCs and their presynaptic partners, and indicate that retinal interneurons regulate the fate of injured RGCs. Importantly, $Zn^{2+}$ chelation has a wide therapeutic window, with chelators continuing to enhance outcome even if introduced several days after nerve damage. The persistent RGC survival, enhancement of the proregenerative effects of *pten* deletion, and clinical feasibility of chelating zinc strongly argue for chelation as a therapeutic strategy. Moreover, even if $Zn^{2+}$ chelation alone is insufficient to restore central connections, long-term preservation of RGCs could have considerable value in enabling a prosthetic device to read out the activity of RGCs transduced to express a fluorescent reporter of activity and represent the code the eye sends to the brain more accurately than reading out the activity of photoreceptors (105). $Zn^{2+}$ chelators are already in clinical use for other purposes (106), and it will be important to determine whether these agents can augment axon regeneration after other types of CNS injury or protect RGCs in neurodegenerative diseases such as glaucoma.

## Methods

**Animal Use, Surgeries, and Intraocular Injections.** Animal studies were performed at Boston Children's Hospital with approval of the Institutional Animal Care and Use Committee. Housing conditions, strains of mice used, and surgical procedures are described in *SI Methods*. Animals were assigned to different treatment groups and, in any given experiment, surgeries were done for several groups at a time. Subsequent processing was performed blinded to treatment. Reagents that were injected intraocularly included the specific $Zn^{2+}$ chelators TPEN [20–500 μM; Calbiochem; $K_d$ for $Zn^{2+} = 2.6 \times 10^{-16}$ M, $K_d$ for $Ca^{2+} = 4 \times 10^{-5}$ M (92)] and ZX1 [10–1,000 μM; $K_d$ for $Zn^{2+}$ = 1.0 nM; no detectable interaction with $Ca^{2+}$ (38)]; Zymosan (12.5 μg/μL; Sigma, sterilized); 8-(4-chlorophenylthio) (CPT)-cAMP (50 μM; Sigma), a membrane permeable, nonhydrolyzable cAMP analog, and TeNT (20 nM; List Biological Laboratories), which cleaves the synaptic vesicle protein synaptobrevin and prevents transmitter release (107). In most cases, the $Zn^{2+}$ chelators TPEN or ZX1 were injected right after NC and 4 d later. In the time-course study, however, we administered single injections at 0, 1, 3, or 5 d after NC. In some groups, to chelate the earliest wave of $Zn^{2+}$ elevation, an additional injection of either chelator was given 1 d before NC (pretreatment). Vehicle-treated controls received PBS alone. To delete the *pten* gene in RGCs, AAV2-Cre ($5 \times 10^{12}$ GC/mL; Vector Laboratories) was injected intraocularly (3 μL) in $pten^{flx/flx}$ mice, 6–8 wk of age, avoiding injury to the lens. In some studies, intraocularly injected AAV2 expressing an mCherry reporter (AAV2-mCherry, $2 \times 10^{12}$ GC/mL; gift from Luk Vandenberghe, Massachusetts Eye and Ear Infirmary and Harvard Medical School, Boston, MA) was used to label RGCs, whereas AAV6-mCherry ($5 \times 10^{12}$ GC/mL; Virovek) was used to label retinal interneurons and their processes in the IPL. Viruses (3 μL per eye) were injected 2 wk before optic nerve surgery to allow for sufficient labeling at the time of NC.

**$Zn^{2+}$ AMG and Quantitation.** The selectivity of AMG for mobile $Zn^{2+}$ is described in *Discussion* and *SI Methods*. Using a modification of a published AMG procedure to visualize mobile $Zn^{2+}$ (60), mice were injected intraperitoneally with sodium selenite ($Na_2SeO_3$, 1.5 mg/mL in distilled $H_2O$; Sigma, 15 mg/kg) and were kept alive for 4 h to allow for optimal zinc-selenite precipitation in vivo, as determined empirically. Our pilot studies showed that we needed to wait at least 2 h after surgery for animals to recover before administering $Na_2SeO_3$, and that we obtained optimal staining in the retina ~4 h after $Na_2SeO_3$ injections. Thus, the minimum survival time after surgery that we could examine with this technique was 6 h. An overdose of anesthesia was then given followed by transcardial perfusion with isotonic saline (Sigma) and 2.5% (vol/vol) glutaraldehyde (GA; Ted Pella) in 0.1 M phosphate buffer (PB; pH 7.4). Details of tissue processing are given in *SI Methods*. To verify the specificity of the AMG signal for zinc, TPEN or ZX1 was injected intraocularly (100 μM, 3 μL per eye) following NC, or PBS was injected as a vehicle control. Five images from different areas of each retinal section were captured under bright-field illumination (600×; E800; Nikon). The intensity of the $Zn^{2+}$-AMG signal in the IPL was analyzed using ImageJ software. $Zn^{2+}$-positive cell numbers in the GCL of each retinal section were determined under light microscopy. AMG staining and imaging were done simultaneously for all samples to be compared with each other. To obtain a representative sampling, we analyzed five areas in each of three to five sections per case with ~150-μm intervals between sections. Average signal intensity as well as $Zn^{2+}$-positive cell numbers were calculated from 6 to 14 individual cases per condition. All images are representative of multiple samples. The small SEMs in $Zn^{2+}$ intensity and cell numbers throughout the study point to a relatively small sampling error.

**$Zn^{2+}$ Fluorescence in Retina and Quantitation of Intensity.** ZP-1 (108) is a highly selective, membrane-permeable, fluorescent probe for $Zn^{2+}$ [$K_d$ for $Zn^{2+}$ = 0.7 ± 0.1 nM with no detectable interaction with $Ca^{2+}$ (32)]. ZP-1 gave a strong, reproducible signal when injected intraocularly and had no apparent

systemic effects. We determined empirically that optimal results were obtained after a 24-h labeling period. Thus, in all cases we injected ZP-1 intraocularly (500 μM, 3 μL per eye) 24 h before killing (e.g., 18 h before surgery to examine $Zn^{2+}$ accumulation 6 h after surgery). Details of tissue processing are in *SI Methods*. Fluorescent images were captured and relative ZP-1 intensity in the IPL of the retina was analyzed using ImageJ software. Average intensities were calculated from five to seven individual cases per condition and images are representative of these results.

**Colocalization with Synaptic Markers.** Standard histological procedures and antibody information are described in *SI Methods*. All tissues to be compared were stained at the same time and all settings were kept constant for imaging. Colocalization analysis was done by ImageJ software using 10 cases from each group. Mander's value (tM) and Pearson's *r* value (*r*) were used to represent the extent of colocalization. All images are representative of signals obtained from multiple cases across two or three independent experiments.

**Quantitation of RGC Survival and Axon Regeneration.** Details are described in *SI Methods*.

**Quantitative Reverse-Transcription PCR.** To investigate molecular events associated with $Zn^{2+}$ elevation, we examined changes in the expression of multiples genes by quantitative PCR (qPCR). Gene names and sequences of primers used for qPCR are shown in Fig. S7*A*. Methods are described in *SI Methods*.

**Immunostaining and Quantitation of Cell Death Markers.** We visualized changes in the expression of representative pro- and antiapoptotic cell death markers with and without $Zn^{2+}$ chelation 5 d after NC. Further details are provided in *SI Methods*.

**Statistical Analyses.** All tissue processing, quantification, and data analysis were done blindly throughout the study. Sample sizes were based on accepted standards in the literature and prior experience from our laboratory. Sample size (*n*) represents total number of biological replicates in each condition across all experiments that were performed ($n \geq 2$) experiments. All experiments contained positive and negative controls and multiple experimental conditions. After establishing the methodology for any type of study, no cases were excluded in our data analysis. Parametric tests (ANOVA with Bonferroni post hoc tests or unpaired Student's *t* tests, two-tailed) were used after determining normality of distribution of data (SPSS v18.0 and Graphpad v6.0). Data are presented as Means ± SEM. All difference were considered significant with $P < 0.05$.

**ACKNOWLEDGMENTS.** We thank Drs. Elias Aizenman (University of Pittsburgh), Elio Raviola (Harvard Medical School), Kathleen Rockland (Boston University), Peter Stys (University of Calgary), and Wei Lin (Massachusetts Institute of Technology) for advice; Dr. Thanos Tzounopoulos (University of Pittsburgh) for ZnT-3 knockout (*slc30a3*$^{-/-}$) mice; Dr. Luk Vandenberghe (Massachusetts Eye and Ear Infirmary/Harvard Medical School) for AAV2-mCherry; Drs. Chinfei Chen and Thomas Schwarz (Boston Children's Hospital/Harvard Medical School) for comments on an early version of the manuscript; Dr. Kush Kapur (Clinical Research Center, Boston Children's Hospital) for statistical guidance; Dr. Anthony Hill (Boston Children's Hospital) for consultation on image analysis; and the Intellectual and Developmental Disabilities Research Center of Boston Children's Hospital (NIH P30 HD018655) for use of the Histology and Image Analysis Cores. This work was supported in part by National Eye Institute Grant 1 R01 EY024481 (to P.A.R. and L.B.); National Institute of Neurological Diseases and Stroke Grant R01NS066019 (to P.A.R.); National Institute of Mental Health Grant R21MH104318 (to P.A.R.); US Department of Defense Grant CDMRP DM102446 (to L.B.); the Dr. Miriam and Sheldon G. Adelson Medical Research Foundation (L.B.); National Institute of General Medical Sciences Grant GM 065519 (to S.J.L.); China Scholarship Council Grant 2010638086 (to Y.L.); Swiss National Science Foundation Grants PBBEB-146099 and PBBEB-155299 (to L.A.); the Uehara Memorial Foundation and Kowa Life Science Foundation (K.Y.); the TAV Airports Holding Life and Education Foundation (B.E.); the Baby Alex Foundation (P.A.R.); and the Humboldt Foundation (U.-P.A.).

1. Chierzi S, Strettoi E, Cenni MC, Maffei L (1999) Optic nerve crush: Axonal responses in wild-type and bcl-2 transgenic mice. *J Neurosci* 19(19):8367–8376.
2. Watkins TA, et al. (2013) DLK initiates a transcriptional program that couples apoptotic and regenerative responses to axonal injury. *Proc Natl Acad Sci USA* 110(10):4039–4044.
3. Welsbie DS, et al. (2013) Functional genomic screening identifies dual leucine zipper kinase as a key mediator of retinal ganglion cell death. *Proc Natl Acad Sci USA* 110(10):4045–4050.
4. Hu Y, et al. (2012) Differential effects of unfolded protein response pathways on axon injury-induced death of retinal ganglion cells. *Neuron* 73(3):445–452.
5. Janssen KT, Mac Nair CE, Dietz JA, Schlamp CL, Nickells RW (2013) Nuclear atrophy of retinal ganglion cells precedes the bax-dependent stage of apoptosis. *Invest Ophthalmol Vis Sci* 54(3):1805–1815.
6. Pelzel HR, Schlamp CL, Nickells RW (2010) Histone H4 deacetylation plays a critical role in early gene silencing during neuronal apoptosis. *BMC Neurosci* 11:62.
7. Fernandes KA, et al. (2012) JNK2 and JNK3 are major regulators of axonal injury-induced retinal ganglion cell death. *Neurobiol Dis* 46(2):393–401.
8. Almasieh M, Wilson AM, Morquette B, Cueva Vargas JL, Di Polo A (2012) The molecular basis of retinal ganglion cell death in glaucoma. *Prog Retin Eye Res* 31(2):152–181.
9. Knöferle J, et al. (2010) Mechanisms of acute axonal degeneration in the optic nerve in vivo. *Proc Natl Acad Sci USA* 107(13):6064–6069.
10. Ribas VT, Koch JC, Michel U, Bähr M, Lingor P (January 5, 2016) Attenuation of axonal degeneration by calcium channel inhibitors improves retinal ganglion cell survival and regeneration after optic nerve crush. *Mol Neurobiol*, 10.1007/s12035-015-9676-2.
11. Baldwin KT, Carbajal KS, Segal BM, Giger RJ (2015) Neuroinflammation triggered by β-glucan/dectin-1 signaling enables CNS axon regeneration. *Proc Natl Acad Sci USA* 112(8):2581–2586.
12. Yin Y, et al. (2003) Macrophage-derived factors stimulate optic nerve regeneration. *J Neurosci* 23(6):2284–2293.
13. Park KK, et al. (2008) Promoting axon regeneration in the adult CNS by modulation of the PTEN/mTOR pathway. *Science* 322(5903):963–966.
14. Smith PD, et al. (2009) SOCS3 deletion promotes optic nerve regeneration in vivo. *Neuron* 64(5):617–623.
15. Moore DL, et al. (2009) KLF family members regulate intrinsic axon regeneration ability. *Science* 326(5950):298–301.
16. Dickendesher TL, et al. (2012) NgR1 and NgR3 are receptors for chondroitin sulfate proteoglycans. *Nat Neurosci* 15(5):703–712.
17. Shen Y, et al. (2009) PTPsigma is a receptor for chondroitin sulfate proteoglycan, an inhibitor of neural regeneration. *Science* 326(5952):592–596.
18. Yin Y, et al. (2006) Oncomodulin is a macrophage-derived signal for axon regeneration in retinal ganglion cells. *Nat Neurosci* 9(6):843–852.
19. Kurimoto T, et al. (2010) Long-distance axon regeneration in the mature optic nerve: Contributions of oncomodulin, cAMP, and pten gene deletion. *J Neurosci* 30(46):15654–15663.
20. Duan X, et al. (2015) Subtype-specific regeneration of retinal ganglion cells following axotomy: Effects of osteopontin and mTOR signaling. *Neuron* 85(6):1244–1256.
21. Yin Y, et al. (2009) Oncomodulin links inflammation to optic nerve regeneration. *Proc Natl Acad Sci USA* 106(46):19587–19592.
22. Müller A, Hauk TG, Leibinger M, Marienfeld R, Fischer D (2009) Exogenous CNTF stimulates axon regeneration of retinal ganglion cells partially via endogenous CNTF. *Mol Cell Neurosci* 41(2):233–246.
23. Li S, et al. (2016) Promoting axon regeneration in the adult CNS by modulation of the melanopsin/GPCR signaling. *Proc Natl Acad Sci USA* 113(7):1937–1942.
24. Lim JH, et al. (2016) Neural activity promotes long-distance, target-specific regeneration of adult retinal axons. *Nat Neurosci* 19(8):1073–1084.
25. Benowitz LI, He Z, Goldberg JL (2015) Reaching the brain: Advances in optic nerve regeneration. *Exp Neurol* 287(Pt 3):365–373.
26. Li S, et al. (2015) Injured adult retinal axons with Pten and Socs3 co-deletion reform active synapses with suprachiasmatic neurons. *Neurobiol Dis* 73:366–376.
27. de Lima S, et al. (2012) Full-length axon regeneration in the adult mouse optic nerve and partial recovery of simple visual behaviors. *Proc Natl Acad Sci USA* 109(23):9149–9154.
28. Kochańczyk T, Drozd A, Krężel A (2015) Relationship between the architecture of zinc coordination and zinc binding affinity in proteins—Insights into zinc regulation. *Metallomics* 7(2):244–257.
29. Ladomery M, Dellaire G (2002) Multifunctional zinc finger proteins in development and disease. *Ann Hum Genet* 66(Pt 5-6):331–342.
30. Kimura T, Kambe T (2016) The functions of metallothionein and ZIP and ZnT transporters: An overview and perspective. *Int J Mol Sci* 17(3):336.
31. Maret W (2015) Analyzing free zinc(II) ion concentrations in cell biology with fluorescent chelating molecules. *Metallomics* 7(2):202–211.
32. Hessels AM, Merkx M (2015) Genetically-encoded FRET-based sensors for monitoring Zn(2+) in living cells. *Metallomics* 7(2):258–266.
33. Qin Y, et al. (2013) Direct comparison of a genetically encoded sensor and small molecule indicator: Implications for quantification of cytosolic Zn(2+). *ACS Chem Biol* 8(11):2366–2371.
34. Choi DW, Koh JY (1998) Zinc and brain injury. *Annu Rev Neurosci* 21:347–375.
35. Koh JY, et al. (1996) The role of zinc in selective neuronal death after transient global cerebral ischemia. *Science* 272(5264):1013–1016.
36. Krapivinsky G, Krapivinsky L, Manasian Y, Clapham DE (2014) The TRPM7 chanzyme is cleaved to release a chromatin-modifying kinase. *Cell* 157(5):1061–1072.
37. Vogt K, Mellor J, Tong G, Nicoll R (2000) The actions of synaptically released zinc at hippocampal mossy fiber synapses. *Neuron* 26(1):187–196.
38. Pan E, et al. (2011) Vesicular zinc promotes presynaptic and inhibits postsynaptic long-term potentiation of mossy fiber-CA3 synapse. *Neuron* 71(6):1116–1126.
39. Vergnano AM, et al. (2014) Zinc dynamics and action at excitatory synapses. *Neuron* 82(5):1101–1114.
40. Kalappa BI, Anderson CT, Goldberg JM, Lippard SJ, Tzounopoulos T (2015) AMPA receptor inhibition by synaptically released zinc. *Proc Natl Acad Sci USA* 112(51):15749–15754.
41. Ripps H, Chappell RL (2014) Review: Zinc's functional significance in the vertebrate retina. *Mol Vis* 20:1067–1074.

42. Kaneda M, Ishii K, Akagi T, Tatsukawa T, Hashikawa T (2005) Endogenous zinc can be a modulator of glycinergic signaling pathway in the rat retina. *J Mol Histol* 36(3): 179–185.
43. Danbolt N (1979) Acrodermatitis enteropathica. *Br J Dermatol* 100(1):37–40.
44. Prasad AS (2012) Discovery of human zinc deficiency: 50 years later. *J Trace Elem Med Biol* 26(2-3):66–69.
45. Dufner-Beattie J, et al. (2003) The acrodermatitis enteropathica gene ZIP4 encodes a tissue-specific, zinc-regulated zinc transporter in mice. *J Biol Chem* 278(35):33474–33481.
46. Engelken J, et al. (2014) Extreme population differences in the human zinc transporter ZIP4 (SLC39A4) are explained by positive selection in Sub-Saharan Africa. *PLoS Genet* 10(2):e1004128.
47. Sensi SL, Paoletti P, Bush AI, Sekler I (2009) Zinc in the physiology and pathology of the CNS. *Nat Rev Neurosci* 10(11):780–791.
48. Frederickson CJ, Koh JY, Bush AI (2005) The neurobiology of zinc in health and disease. *Nat Rev Neurosci* 6(6):449–462.
49. Granzotto A, Sensi SL (2015) Intracellular zinc is a critical intermediate in the excitotoxic cascade. *Neurobiol Dis* 81:25–37.
50. Medvedeva YV, Lin B, Shuttleworth CW, Weiss JH (2009) Intracellular Zn2+ accumulation contributes to synaptic failure, mitochondrial depolarization, and cell death in an acute slice oxygen-glucose deprivation model of ischemia. *J Neurosci* 29(4):1105–1114.
51. Shuttleworth CW, Weiss JH (2011) Zinc: New clues to diverse roles in brain ischemia. *Trends Pharmacol Sci* 32(8):480–486.
52. Shah NH, Aizenman E (2014) Voltage-gated potassium channels at the crossroads of neuronal function, ischemic tolerance, and neurodegeneration. *Transl Stroke Res* 5(1):38–58.
53. Sensi SL, et al. (2011) The neurophysiology and pathology of brain zinc. *J Neurosci* 31(45):16076–16085.
54. Bush AI (2013) The metal theory of Alzheimer's disease. *J Alzheimers Dis* 33(Suppl 1): S277–S281.
55. Estévez AG, et al. (1999) Induction of nitric oxide-dependent apoptosis in motor neurons by zinc-deficient superoxide dismutase. *Science* 286(5449):2498–2500.
56. Bahadorani S, et al. (2013) Expression of zinc-deficient human superoxide dismutase in *Drosophila* neurons produces a locomotor defect linked to mitochondrial dysfunction. *Neurobiol Aging* 34(10):2322–2330.
57. Williams JR, et al. (2016) Copper delivery to the CNS by CuATSM effectively treats motor neuron disease in SOD(G93A) mice co-expressing the Copper-Chaperone-for-SOD. *Neurobiol Dis* 89:1–9.
58. Aras MA, Aizenman E (2011) Redox regulation of intracellular zinc: Molecular signaling in the life and death of neurons. *Antioxid Redox Signal* 15(8):2249–2263.
59. Zhang Y, Aizenman E, DeFranco DB, Rosenberg PA (2007) Intracellular zinc release, 12-lipoxygenase activation and MAPK dependent neuronal and oligodendroglial death. *Mol Med* 13(7-8):350–355.
60. Wang X, Wang ZY, Gao HL, Danscher G, Huang L (2006) Localization of ZnT7 and zinc ions in mouse retina—Immunohistochemistry and selenium autometallography. *Brain Res Bull* 71(1-3):91–96.
61. Danscher G, Stoltenberg M (2005) Zinc-specific autometallographic in vivo selenium methods: Tracing of zinc-enriched (ZEN) terminals, ZEN pathways, and pools of zinc ions in a multitude of other ZEN cells. *J Histochem Cytochem* 53(2):141–153.
62. Danscher G, Nørgaard JO, Baatrup E (1987) Autometallography: Tissue metals demonstrated by a silver enhancement kit. *Histochemistry* 86(5):465–469.
63. Ugarte M, Osborne NN (2001) Zinc in the retina. *Prog Neurobiol* 64(3):219–249.
64. Cen LP, et al. (2015) Bilateral retinal microglial response to unilateral optic nerve transection in rats. *Neuroscience* 311:56–66.
65. Lees GJ, Cuajungco MP, Leong W (1998) Effect of metal chelating agents on the direct and seizure-related neuronal death induced by zinc and kainic acid. *Brain Res* 799(1):108–117.
66. Huang Z, Lippard SJ (2012) Illuminating mobile zinc with fluorescence from cuvettes to live cells and tissues. *Methods Enzymol* 505:445–468.
67. Wang Z, Li JY, Dahlström A, Danscher G (2001) Zinc-enriched GABAergic terminals in mouse spinal cord. *Brain Res* 921(1-2):165–172.
68. Palmiter RD, Cole TB, Quaife CJ, Findley SD (1996) ZnT-3, a putative transporter of zinc into synaptic vesicles. *Proc Natl Acad Sci USA* 93(25):14934–14939.
69. Wang ZY, Danscher G, Dahlström A, Li JY (2003) Zinc transporter 3 and zinc ions in the rodent superior cervical ganglion neurons. *Neuroscience* 120(3):605–616.
70. Masland RH (2001) The fundamental plan of the retina. *Nat Neurosci* 4(9):877–886.
71. Redenti S, Chappell RL (2007) Müller cell zinc transporter-3 labeling suggests a role in outer retina zinc homeostasis. *Mol Med* 13(7-8):376–379.
72. Redenti S, Chappell RL (2004) Localization of zinc transporter-3 (ZnT-3) in mouse retina. *Vision Res* 44(28):3317–3321.
73. Hellström M, et al. (2009) Cellular tropism and transduction properties of seven adeno-associated viral vector serotypes in adult retina after intravitreal injection. *Gene Ther* 16(4):521–532.
74. Klimczak RR, Koerber JT, Dalkara D, Flannery JG, Schaffer DV (2009) A novel adeno-associated viral variant for efficient and selective intravitreal transduction of rat Müller cells. *PLoS One* 4(10):e7467.
75. Cui Q, Yip HK, Zhao RC, So KF, Harvey AR (2003) Intraocular elevation of cyclic AMP potentiates ciliary neurotrophic factor-induced regeneration of adult rat retinal ganglion cell axons. *Mol Cell Neurosci* 22(1):49–61.
76. Kermer P, et al. (2000) Caspase-9: Involvement in secondary death of axotomized rat retinal ganglion cells in vivo. *Brain Res Mol Brain Res* 85(1-2):144–150.
77. Isenmann S, Wahl C, Krajewski S, Reed JC, Bähr M (1997) Up-regulation of Bax protein in degenerating retinal ganglion cells precedes apoptotic cell death after optic nerve lesion in the rat. *Eur J Neurosci* 9(8):1763–1772.
78. Leon S, Yin Y, Nguyen J, Irwin N, Benowitz LI (2000) Lens injury stimulates axon regeneration in the mature rat optic nerve. *J Neurosci* 20(12):4615–4626.
79. Goldberg JL, Klassen MP, Hua Y, Barres BA (2002) Amacrine-signaled loss of intrinsic axon growth ability by retinal ganglion cells. *Science* 296(5574):1860–1864.
80. Schwab ME (2004) Nogo and axon regeneration. *Curr Opin Neurobiol* 14(1):118–124.
81. Fitch MT, Silver J (2008) CNS injury, glial scars, and inflammation: Inhibitory extracellular matrices and regeneration failure. *Exp Neurol* 209(2):294–301.
82. Sun F, He Z (2010) Neuronal intrinsic barriers for axon regeneration in the adult CNS. *Curr Opin Neurobiol* 20(4):510–518.
83. Coleman JE (1992) Zinc proteins: Enzymes, storage proteins, transcription factors, and replication proteins. *Annu Rev Biochem* 61:897–946.
84. Berg JM, Shi Y (1996) The galvanization of biology: A growing appreciation for the roles of zinc. *Science* 271(5252):1081–1085.
85. Tonkin EG, Valentine HL, Milatovic DM, Valentine WM (2004) N,N-diethyldithiocarbamate produces copper accumulation, lipid peroxidation, and myelin injury in rat peripheral nerve. *Toxicol Sci* 81(1):160–171.
86. Garner B, Roberg K, Qian M, Eaton JW, Truscott RJ (2000) Distribution of ferritin and redox-active transition metals in normal and cataractous human lenses. *Exp Eye Res* 71(6):599–607.
87. Holm IE, Andreasen A, Danscher G, Pérez-Clausell J, Nielsen H (1988) Quantification of vesicular zinc in the rat brain. *Histochemistry* 89(3):289–293.
88. Danscher G, Stoltenberg M, Bruhn M, Søndergaard C, Jensen D (2004) Immersion autometallography: Histochemical in situ capturing of zinc ions in catalytic zinc-sulfur nanocrystals. *J Histochem Cytochem* 52(12):1619–1625.
89. Nolan EM, Lippard SJ (2009) Small-molecule fluorescent sensors for investigating zinc metalloneurochemistry. *Acc Chem Res* 42(1):193–203.
90. Golovine K, et al. (2008) Depletion of intracellular zinc increases expression of tumorigenic cytokines VEGF, IL-6 and IL-8 in prostate cancer cells via NF-kappaB-dependent pathway. *Prostate* 68(13):1443–1449.
91. Hyun HJ, et al. (2001) Depletion of intracellular zinc and copper with TPEN results in apoptosis of cultured human retinal pigment epithelial cells. *Invest Ophthalmol Vis Sci* 42(2):460–465.
92. Arslan P, Di Virgilio F, Beltrame M, Tsien RY, Pozzan T (1985) Cytosolic Ca2+ homeostasis in Ehrlich and Yoshida carcinomas. A new, membrane-permeant chelator of heavy metals reveals that these ascites tumor cell lines have normal cytosolic free Ca2+. *J Biol Chem* 260(5):2719–2727.
93. Cole TB, Wenzel HJ, Kafer KE, Schwartzkroin PA, Palmiter RD (1999) Elimination of zinc from synaptic vesicles in the intact mouse brain by disruption of the ZnT3 gene. *Proc Natl Acad Sci USA* 96(4):1716–1721.
94. Hoch E, et al. (2012) Histidine pairing at the metal transport site of mammalian ZnT transporters controls Zn2+ over Cd2+ selectivity. *Proc Natl Acad Sci USA* 109(19): 7202–7207.
95. Kolb H (1995) Inner plexiform layer. *Webvision: The Organization of the Retina and Visual System*, eds Kolb H, Fernandez E, Nelson R (Univ of Utah Health Science Center, Salt Lake City).
96. Masland RH (2012) The neuronal organization of the retina. *Neuron* 76(2):266–280.
97. Land PW, Aizenman E (2005) Zinc accumulation after target loss: An early event in retrograde degeneration of thalamic neurons. *Eur J Neurosci* 21(3):647–657.
98. Danscher G, et al. (2001) Inhibitory zinc-enriched terminals in mouse spinal cord. *Neuroscience* 105(4):941–947.
99. Paoletti P, Ascher P, Neyton J (1997) High-affinity zinc inhibition of NMDA NR1-NR2A receptors. *J Neurosci* 17(15):5711–5725.
100. Hwang JJ, Park MH, Choi SY, Koh JY (2005) Activation of the Trk signaling pathway by extracellular zinc. Role of metalloproteinases. *J Biol Chem* 280(12):11995–12001.
101. Yang J, et al. (2015) Pathological axonal death through a MAPK cascade that triggers a local energy deficit. *Cell* 160(1-2):161–176.
102. Aravindakumar CT, Ceulemans J, De Ley M (1999) Nitric oxide induces Zn2+ release from metallothionein by destroying zinc-sulphur clusters without concomitant formation of S-nitrosothiol. *Biochem J* 344(Pt 1):253–258.
103. Rivera-Fuentes P, Lippard SJ (2015) Metal-based optical probes for live cell imaging of nitroxyl (HNO). *Acc Chem Res* 48(11):2927–2934.
104. Li Y, et al. (2015) Presynaptic zinc regulates optic nerve regeneration: Role of ZnT-3 and nNOS. *2015 Neuroscience Meeting Planner* (Society for Neuroscience, Chicago, IL), Program No. 568.02. Available at www.abstractsonline.com/Plan/ViewAbstract.aspx?sKey=bec77ba2-7da8-43b3-a991-bf25a0d962f4&cKey=f09f184e-083b-43df-9a68-49c6bcbb01ab&mKey=%7bD0FF4555-8574-4FBB-B9D4-04EEC8BA0C84%7d. Accessed December 13, 2016.
105. Nirenberg S, Pandarinath C (2012) Retinal prosthetic strategy with the capacity to restore normal vision. *Proc Natl Acad Sci USA* 109(37):15012–15017.
106. Cherny RA, et al. (2001) Treatment with a copper-zinc chelator markedly and rapidly inhibits beta-amyloid accumulation in Alzheimer's disease transgenic mice. *Neuron* 30(3):665–676.
107. Pellizzari R, Rossetto O, Schiavo G, Montecucco C (1999) Tetanus and botulinum neurotoxins: Mechanism of action and therapeutic uses. *Philos Trans R Soc Lond B Biol Sci* 354(1381):259–268.
108. Burdette SC, Walkup GK, Spingler B, Tsien RY, Lippard SJ (2001) Fluorescent sensors for Zn(2+) based on a fluorescein platform: synthesis, properties and intracellular distribution. *J Am Chem Soc* 123(32):7831–7841.
109. Guo X, Snider WD, Chen B (2016) GSK3β regulates AKT-induced central nervous system axon regeneration via an eIF2Bε-dependent, mTORC1-independent pathway. *eLife* 5:e11903.
110. Benowitz LI, et al. (1988) Anatomical distribution of the growth-associated protein GAP-43/B-50 in the adult rat brain. *J Neurosci* 8(1):339–352.